Title (max 150 characters): Relationship between cortical state and spiking activity in lateral geniculate nucleus of anaesthetised marmosets

Running title (max 70 chars): Cortical state and LGN spikes

Authors: Alexander N.J. Pietersen[a,b], Soon Keen Cheong[a,b], Brandon Munn[a,e], Pulin Gong[a,e], Paul R. Martin[a,b,c], Samuel G. Solomon[a,c]

[a] Australian Research Council Centre of Excellence for Integrative Brain Function, University of Sydney, Australia, 2006

[b] Save Sight Institute, University of Sydney Eye Hospital Campus, Sydney, Australia, 2001

[c] School of Medical Sciences, University of Sydney, Sydney, Australia, 2006

[d] Department of Experimental Psychology, University College London, United Kingdom, WC1H 0AP

[e] School of Physics, University of Sydney, Sydney, Australia, 2006

email addresses in order: alexander.pietersen@sydney.edu.au, kcheong@mail.cvs.rochester.edu, bmun7133@uni.sydney.edu.au, p.gong@physics.usyd.edu.au, s.solomon@ucl.ac.uk, prmartin@physiol.usyd.edu.au.

Corresponding Author: P. R. Martin, email: prmartin@physiol.usyd.edu.au, phone: +61 2 9382 7539, Postal address: Sydney Eye Hospital Campus C09, 8 Macquarie St, Sydney 2001, Australia.

Key words: Visual pathways, lateral geniculate nucleus, cerebral cortex

This is an Accepted Article that has been peer-reviewed and approved for publication in the The Journal of Physiology, but has yet to undergo copy-editing and proof correction. Please cite this article as an 'Accepted Article'; doi: 10.1113/JP273569.

Table of Contents category: Neuroscience - Behavioural / systems / cognitive

Abstract (max 250 words)

The major afferent cortical pathway in the visual system passes through the dorsal lateral geniculate nucleus (LGN), where nerve signals originating in the eye can first interact with brain circuits regulating visual processing, vigilance, and attention. Here we asked how on-going and visually driven activity in magnocellular (M), parvocellular (P), and koniocellular (K) layers of the LGN are related to cortical state. We recorded extracellular spiking activity in the LGN simultaneously with local field potentials (LFP) in primary visual cortex, in sufentanil-anesthetized marmoset monkeys. We found that asynchronous cortical states (marked by low power in delta-band LFPs) are linked to high spike rates in K cells (but not P cells or M cells), on multi-second timescales. Cortical asynchrony precedes the increases in K cell spike rates by 1–3 s, implying causality. At sub-second timescales, the spiking activity in many cells of all (M, P, and K) classes is phase-locked to delta waves in the cortical LFP, and more cells are phase-locked during synchronous cortical states than during asynchronous cortical states. The switch from low-to-high spike rates in K cells does not degrade their visual signalling capacity. To the contrary, during asynchronous cortical states the fidelity of visual signals transmitted by K cells is improved, likely because K cell responses become less rectified. Overall the data show that slow fluctuations in cortical state are selectively linked to K pathway spiking activity, whereas delta-frequency cortical oscillations entrain spiking activity throughout the entire LGN, in anaesthetised marmosets.

Key points summary (150 words, max 5 points):

• How parallel are the primate visual pathways? In the present study we show that parallel visual pathways in the dorsal lateral geniculate nucleus (LGN) show distinct patterns of interaction with rhythmic activity in primary visual cortex (V1).

• In V1 of anaesthetised marmosets, the electroencephalogram (EEG) frequency spectrum undergoes transient changes that are characterized by fluctuations in delta-band EEG power.

• We show that on multi-second timescales, spiking activity in an evolutionary primitive (koniocellular) LGN pathway is specifically linked to these slow EEG spectrum changes. By contrast, on sub-second (delta frequency) timescales, cortical oscillations can entrain spiking activity throughout the entire LGN.

• Our results are consistent with the hypothesis that in waking animals the koniocellular pathway selectively participates in brain circuits controlling vigilance and attention.

Abbreviations list

AUC, area under the curve

CRT, cathode ray tube

EEG, electroencephalogram

K, Koniocellular

K-bon, koniocellular blue-on/yellow off

LFP, local field potential

LGN, Lateral Geniculate Nucleus

M, Magnocellular

ML, medium/long-wave sensitive

P, Parvocellular

ROC, receiver operator characteristic

S, short-wave sensitive

SD, standard deviation

V1, primary visual cortex (area 17)

Introduction.

The magnocellular (M), parvocellular (P) and koniocellular (K) pathways form three cortical afferent visual streams in primates (reviewed by Casagrande, 1994; Hendry and Reid, 2000; Nassi and Callaway, 2009). Visual signals are considered to travel in parallel on these three streams through the LGN *en route* to the visual cortex (V1), where cortical circuits can use these inputs to extract complex features from the visual image.

In addition to receiving this feed-forward visual signal flow, both LGN and V1 are connected to brainstem centres regulating vigilance and sleep-wake cycles (Bickford et al., 2000; Steriade, 2003; Sherman and Guillery, 2006; Jones, 2007). Further, there are substantial reciprocal projections from layer 6 of V1 to LGN. These projections can exert direct and indirect (*via* the thalamic reticular nucleus) influence on LGN cells (Sherman and Guillery, 2006; Sherman, 2016). Finally, and most importantly, the intrinsic circuitry of V1 generates oscillatory states ranging from synchronous (coherent low-frequency activity) to asynchronous (less coherent; reviewed by Buzsáki and Draguhn, 2004; Wang, 2010). Unsurprisingly therefore, studies in rodents, primates and carnivores agree that thalamocortical pathways exhibit brain state-dependent changes in activity, across a range of electroencephalogram (EEG) band frequencies (McCormick et al., 1992; Contreras and Steriade, 1995; Destexhe et al., 1998; Crunelli and Hughes, 2010; Zagha and McCormick, 2014).

Briggs and Usrey (2009) showed that direct reciprocal pathways from cortex to LGN are organized in parallel with properties analogous to the M, P, and K input streams. This result

implies that thalamocortical loops comprise independent parallel subsystems, as illustrated schematically in Figure 1A. But a different possibility is suggested by studies in comparative anatomy. The K stream is part of an evolutionary ancient group of thalamo-cortical pathways including, for example, paralemniscal somatosensory and tegmental auditory pathways . (reviewd by Casagrande, 1994; Jones, 2001; Jones, 2007). The cortical projections of K cells are more diverse and widespread than those of P and M cells, and projection targets of K cells include supragranular layers of primary visual cortex as well as extrastriate cortices (Fitzpatrick et al., 1983; Casagrande, 1994; Sincich et al., 2004; Casagrande et al., 2007; Jones, 2007; Warner et al., 2010). These anatomical features imply that cortical activity generated by K pathways could feed into activity generated by P and M pathways, as shown schematically in Figure 1B.

In sufentanil-anaesthetized marmosets, V1 displays infrequent and short-lived periods of asynchronous (low delta-power) EEG activity (Cheong et al., 2011). These V1 state changes are analogous to changes seen when awake animals move from inattentive to attentive states. We previously showed that K cells (but not P cells or M cells), show coherent slow sustained increases in spike discharge rate (Cheong et al., 2011). Here we use time-series analyses and visual stimuli to study the temporal relation between V1 state and coherent activity in LGN. We also ask whether and how V1 state can influence visual signal transmission through the LGN.

Materials and Methods

Ethical approval.

Procedures were approved by institutional (University of Melbourne and University of Sydney) Animal Experimentation and Ethics Committees. Procedures conform to the Society for Neuroscience and Australian National Health and Medical Research Council policies on the use of animals in neuroscience research, and to Journal of Physiology reporting guidelines

(Grundy, 2015).

Animal preparation.

Extracellular recordings were made from the LGN of 13 adult marmosets (*Callithrix jacchus*, weight range 335 – 420 g) obtained from the Australian National Non-Human Primate Breeding Facility in Gippsland, VIC, Australia. Visual evoked response properties of many cells from these animals were previously published (Cheong et al., 2013; Cheong and Pietersen, 2014; Pietersen et al., 2014); all responses were reanalysed for the present study. Anaesthesia was induced by intramuscular injection of 12 mg kg^{-1} Alfaxan (Jurox, NSW, AUS), and 3 mg kg^{-1} diazepam (Roche, NSW, AUS). During surgery anaesthesia levels were maintained with supplementary doses of Alfaxan. Local anaesthesia (Xylocaine 2%; AstraZeneca, NSW, Australia) was applied to surgery sites. A tail vein was cannulised, and an endotracheal tube inserted. The animal was placed in a stereotaxic frame, and craniotomies were made over the right LGN and primary visual cortex. Animals were artificially respired with a 70%: 30% mixture of NO_2: Carbogen (5% CO_2 in O_2). Anaesthesia and analgesia were maintained during recording by intravenous sufentanil citrate infusion (6–30 μg kg^{-1} h^{-1}; Sufenta Forte, Janssen Cilag, Beerse, BEL) in physiological solution (sodium lactate, Baxter International, NSW, AUS) with added dexamethasone (0.4 kg h^{-1}; Mayne Pharma, VIC, AUS) and Synthamin 17 (amino acids 10%; 225 mg kg^{-1} h^{-1}; Baxter International, NSW, AUS). Following establishment of a stable anaesthetic plane, pancuronium bromide (0.3 kg h^{-1}; AstraZeneca, NSW, AUS) was added to the infusion solution to induce and maintain muscular paralysis. The respiratory depressant effect of Sufentanil obviated the need for a loading dose of paralytic. The animal was artificially ventilated so as to keep the end-tidal CO_2 close to 3.7%. Electroencephalogram and electrocardiogram signals were monitored to ensure adequate anaesthesia levels. Dominance of low frequencies (< 10 Hz) in the EEG recording, and stability of the EEG frequency spectrum

under intermittent noxious stimulus (toe-pinch) were taken as indication of adequate anaesthesia. We found that low sufentanil dose rates in the range cited above were always very effective during the first 24 h of recordings. Thereafter, drifts towards higher frequencies (> 10 Hz) in the EEG record were counteracted by increasing the rate of venous infusion or the concentration of anesthetic. Typical duration of a recording session was 72–94 hours. Rectal temperature was kept near 37.0°C with a thermistor-controlled heating blanket. An hourly log of the vital signs described above was maintained. Daily additional antibiotics (80–120 mg kg^{-1} procaine penicillin, Norocillin SA, Norbrook, UK) were injected intramuscularly. Pupils were dilated with phenylephrine hydrochloride (minims 10%, Chauvin Pharmaceuticals, Kingston-upon-Thames, Surrey, UK). Corneas were protected with gas-permeable contact lenses that normally remained in place for the duration of the experiment. Supplementary lenses (with power determined by maximizing the spatial resolution of the first receptive fields encountered for each eye) were used to focus the eyes at a distance of 114 cm. As previously reported (Buzás et al., 2006) we saw little evidence for drifts in eye position or refractive state over the duration of the experiment.

Recording procedures

A recording electrode (parylene-insulated stainless steel, 5 – 11 MΩ, FHC Inc., Bowdoin, Maine, USA), was lowered into the LGN through a guide tube using a hydraulic micropositioner (David Kopf model 640). Action potential waveforms of single cells were discriminated by principal component analysis of amplified voltage signals. Extracellular spike events were captured at 100 μs resolution using a Power Mac G5 running open-source data acquisition software (EXPO/OpenGL; P. Lennie, Rochester, NY).

Bipolar electrodes, constructed from 0.05 mm diameter lacquer-insulated nickel-chromium wire, were inserted into V1 to record local field potentials (LFP). Each electrode had

a vertical tip separation of approximately 0.5 mm. The band-pass filtered LFP (0.3–300 Hz) signal was amplified and displayed on a digital storage oscilloscope (Tektronix DPO2014, Beaverton, OR, USA). A large uniform achromatic flashing stimulus was presented and electrodes were advanced until clear stimulus-locked modulation of the LFP was evident. Histological reconstruction (see below) showed the lower tip of the electrode was typically ~1.0 mm below the cortical surface. The LFP was displayed and saved simultaneously with the raw spike signal recorded in the LGN on the oscilloscope in epochs of 40 s at sample rate 3.125 kHz.

Visual stimuli.

A front-silvered gimballed mirror was used to bring the receptive field onto the centre of a cathode ray tube (CRT) monitor (Sony G520, 100 Hz refresh rate). For each phosphor the relationship between the output of the video card and the photopic luminance was determined. The inverse of this relationship was applied to the signals that were sent to the video card. Visual stimuli were generated using the same computer and software that collected spike waveforms. Stimuli were presented on a grey background (guns set to half-maximum intensity) at mean luminance close to 50 cd m^{-2} and mean chromaticity x=0.361, y=0.363. Visual stimuli were presented through the dominant eye only. Stimuli were placed as close as practicable to the centre of the screen in order to reduce latency variation due to the CRT beam fly-time.

Visual stimuli comprised drifting (5Hz) sine-wave achromatic and cone-isolating gratings of variable spatial frequency and contrast (stimulus duration 2 s; inter-stimulus interval 2.5 s; 20–60 cycles presented), and temporal square-wave intensity and/or chromaticity modulation of a spatially uniform circular field (*pulse*, duration 200 ms; 100 repetitions; inter-stimulus interval 600 ms). Field size for grating and pulsed stimuli was 1–8 degree diameter. Short-wave sensitive (S) and medium/long-wave sensitive (ML) cone-isolating pulses and gratings were constructed by convolving marmoset cone spectral sensitivity with the

spectral distribution of the monitor phosphors (Tailby et al., 2008; Pietersen et al., 2014). During measurement of maintained activity the screen was held at the mean luminance. Between 8 and 20 epochs of data were recorded, each of 40 s duration, with 20 s inter-epoch interval.

Cell classification and histological reconstruction

The P, M, and K cells were distinguished by their responses to the stimuli described above. The P cells show sustained response to maintained contrast and linear contrast-response function. The M cells show transient response to maintained contrast, saturating contrast response function, and response phase advance from intermediate to high contrast levels (Wiesel and Hubel, 1966; Dreher et al., 1976; Kaplan and Shapley, 1986; Kaplan and Benardete, 2001). The K cells showed a variety of response properties including colour-selective "blue-on" (K-bon), "blue-off" (K-boff), "orientation-selective" (K-o) cells and "suppressed-by-contrast" (K-sbc) receptive fields (Martin et al., 1997; Szmajda et al., 2006; Tailby et al., 2007; Roy et al., 2009; Cheong et al., 2013). The majority of K cells included in this report (43/60, 71%) are K-bon cells.

At the conclusion of the experiment an intravenous overdose of 120 mg kg^{-1} pentobarbital sodium (Lethabarb, Vibac, Australia) was given then the animal was transcardially perfused with 0.9% saline followed by 4% paraformaldehyde. Recording track location was reconstructed as described in detail in our previous studies (White et al., 2001; Szmajda et al., 2008). Anatomical location was confirmed for 55% (70/128) of cells. In cases where track location was not determined the receptive field properties, eye dominance, encounter position, and response characteristics described above were used as criteria.

Based on the combined anatomical and physiological criteria described above, one K cell was in the (ventral-most) layer K1, two cells were in K2 (between the M layers), 11 cells were in K3 (between the M and P layers), and 13 were in K2 (between the internal and external P

layers). Two K cells were located 'ectopically' in P layers and two in M layers . The laminar location of 15 K cells could not be determined unequivocally.

Colour vision phenotype

The red-green colour vision phenotype was estimated during the recording session from the pattern of responses to red-green contrast varying stimuli as described in detail elsewhere(Blessing et al., 2004; Forte et al., 2006). Four animals (three male, one female) showed 543 nm dichromatic phenotype; four animals (three male, one female) showed 556 nm dichromatic phenotype; one male animal showed 563 nm dichromatic phenotype; one female animal showed 556/563 nm trichromatic phenotype. The phenotype of the remaining three animals (one male, two female) could not be determined with confidence because insufficient tests were run. No clear differences in the results presented hereinafter were seen on comparing male and female animals, or on comparing dichromatic animals with the single trichromatic animal.

Data analysis.

Off-line analysis was performed using Matlab (2014a, MathWorks, Natick, MA, USA). Spectral power in V1 LFP was estimated by multi-taper analysis (taper parameter 10; moving window width 3 s, step size 0.3 s) using the Chronux toolbox for Matlab (Bokil et al., 2010). Power was normalized to the mean power between 80–100 Hz, and average power for each frequency band (delta: 1–4 Hz, theta: 5–8 Hz, alpha: 8–12 Hz, and beta: 12–30 Hz) was calculated. The filtered signal was classified as showing high delta power (also referred to hereinafter as *synchronous cortical state*) if the RMS delta power was more than 2 SD above the mean value for > 3 s, and low delta power (also referred to hereinafter as *asynchronous cortical state*) otherwise. The reader should note that because we are recording from anaesthetised animals the EEG frequency spectrum is biased to sub-gamma frequencies . (Steriade, 2003; Buzsáki and Draguhn,

2004). Thus our definition of asynchronous cortical state includes more low-frequency power than would be expected in studies of waking brain activity.

Maintained spike rates for P, M, and K cells were calculated using the same moving window parameters as for LFP analysis. Spike phase was analysed by taking the instantaneous phase from the Hilbert transform of filtered delta LFP at the time of spike occurrence (Le Van Quyen et al., 2001). Rayleigh's test for non-uniformity of circular data was used to estimate strength of phase locking (Berens, 2009). The timing of LGN cell spike rate and V1 delta frequency power was subjected to Granger causality analysis using the *bsmart* toolbox for Matlab (Cui et al., 2008). A transition from low to high LGN spike rate was defined as a spike rate increase of at least 20 imp s^{-1} for at least 2 seconds. Spike rate and delta frequency power were first z-scored, then Granger causality was measured using model order of 3 (derived by Akaike information criterion).

The relationship between K cell spike rate and responses to high contrast stimuli were measured using pulse stimuli and receiver operator characteristic (ROC) analysis. Performance curves for ROC analysis were generated by comparing mean spike rate in 350 ms before and 200 ms following stimulus onset. Area under the curve (AUC) of the generated curve was taken as a measure of performance (Bradley, 1997).

Statistics.

Data are presented as mean ± standard deviation unless stated otherwise. Multiple group comparisons were made using Kruskal-Wallis non-parametric analysis of variance with post-hoc K-Bonferroni-corrected multiple pairwise comparison (Matlab functions *kruskalwallis* and *multcompare*). These tests are referred to as *Kruskal-Wallis* and *Multcompare* hereinafter. Two-group comparisons were made using the Wilcoxon non-parametric rank sum test. This test is referred to as *Wilcoxon test* hereinafter. All *p* values are reported with two decimal places.

Results

Spike rate characteristics of P, M and K cells.

Responses of 128 LGN cells (43 P, 25 M, 60 K) are reported. Not all cells were used in every analysis. Figure 2 shows examples of visually evoked and maintained discharge properties of P, M, and K cells. The most readily characterized K cell type in macaque and marmoset monkeys is the blue-on/yellow off (K-bon) cell class (White et al., 1998; Szmajda et al., 2006; Roy et al., 2009); accordingly the majority of K cells included in this report (43/60, 71%) are K-bon cells. Figure 2A shows for a K-bon cell the responses to pulse stimuli (left) and a spatial frequency tuning curve for S-cone isolating gratings. This cell shows response properties typical for K-bon cells including vigorous response to S-cone contrast increments, complete response suppression to ML-cone contrast increments, and mild band-pass spatial tuning for S-cone gratings (White et al., 1998; Tailby et al., 2008). Figure 2B shows responses of an M cell in the same format as Figure 2A; this cell shows vigorous responses to achromatic and ML-cone increments, is weakly suppressed by S-cone increments, and shows saturating contrast-response function (Fig. 2B right, inset panel) for achromatic gratings. The P-off cell (Fig. 2C) shows maintained responses to achromatic contrast decrements, negligible response to S-cone decrements, and linear contrast sensitivity for achromatic gratings.

Figure 2D–F shows recordings where these example cells were presented with a uniform grey screen (~50 cd m^{-2}). The upper traces show local field potential, band-pass filtered for delta frequencies (1–4 Hz). The vertical tick marks represent individual action potentials; the lower histograms show PSTHs of spike rates in 0.5 second bins. Around 15 seconds into the K cell recording, the spike rate increases markedly for about 10 seconds (start marked with arrow). This increase is associated with reduced cortical synchrony, as indicated by the reduction of delta-band amplitude in V1. Comparable changes in cortical synchrony have little or no effect on on-going activity of the M cell (Fig. 2E) or the P cell (Fig. 2F).

Figure 3 shows that as a population, K cells show comparable mean rate (Fig. 3A) but higher spike rate variability (Fig. 3B) than M cells (Fig. 3C) and P cells (Fig. 3D). For K cells, the average SD = 5.1 ± 4.0; for M cells, average SD = 3.1 ± 1.7; for P cells, average SD = 2.7 ± 1.3, *Kruskal-Wallis p* = 0.00). For example, almost half (19/45, 42%) of K cells show SD greater than 5 impulses per second whereas only 3/43 (7%) of P cells and 4/25 (16%) of M cells do. Consistently, a K-means cluster analysis (Matlab statistics toolbox) divides the K cell recordings into two groups with low (<5 imp s^{-1}) and high (> 5 imp s^{-1}) SD (data not shown). This division could indicate the existence of discrete K cell classes with high or low intrinsic variability. More likely however (as we show below) is that changes of V1 state occurred during some K-cell recordings but not during others. Consistent with our previous report (Cheong et al., 2011), across the P, M and K cells sampled we found no significant differences in average maintained spike rate (Fig. 2A) between the three classes (K, 11.4 ± 7.1, n = 45; M, 11.6 ± 6.1, n = 25; P, 9.0 ± 4.6, n = 43; *Kruskal-Wallis p* = 0.15). In the following section we examine the relationship between LGN cell spike rate and delta-band power in V1 in more detail.

K cell spike rate fluctuations correlate with cortical synchrony

Figure 4A shows an example 40 s recording, with spectral analysis of V1 LFP (upper panel), K cell spike rate (centre panel), and the average power ratio (lower panel) over the delta (1–4 Hz, blue), theta (5–8 Hz, green), alpha (8–12 Hz, red) and beta (12–30 Hz, cyan) frequency bands. Power in each frequency band was normalized to the average power between 80 Hz and 100 Hz. The lack of power in V1 LFP (lack of warm colours) above 10 Hz is consistent with deep surgical anaesthesia. Just before the 15 second mark the K cell spike rate increases markedly. This increase is accompanied by reduced cortical synchrony, indicated by 1) a loss of power in the lower frequency bands (lack of warm colours in the heat map), and 2) reduction in the LFP ratios, most noticeably in the delta band. We restricted our analysis to the relation of delta band

power to LGN spike rates, but inspection of Fig. 4A shows that weaker relations of spike rate to other LFP frequency bands may also be present.

For each cell, between 8 and 20 epochs (each of 40 s duration, see Material and Methods) were recorded. Figure 4B-E show scatter plots for four example LGN cells with spike rate on the x-axis and the simultaneously recorded delta frequency LFP ratio on the y-axis. All these cells showed high overall variability in spike rate (SD > 5). The K cells show a negative overall correlation, whereby LGN cell spike rate is high when V1 is in asynchronous state. The K cell in Figure 4B (K-bon cell) shows a systematic decline in LFP ratio with increasing spike rates. The K cell in Figure 4C (K blue-off [K-bof] cell) by contrast shows two distinct modes in spike rate. Of 19 K cells that that displayed high variability in spike rate (SD > 5), 16 showed a significant negative correlation with delta power ($p < 0.01$, Pearson correlation). The example M (Figure 4D) and P (Figure 4E) cells show no clear relation to cortical state, despite the fact that these two cells showed, respectively, the greatest variability of all M and P cells in our dataset. The distribution of correlation coefficients derived from linear regression of LGN cell spike rate and delta LFP ratio is shown in Figure 4F (P– and M-cells) and Figure 4G (K-cells). Here, grey bars show cells with a significant correlation; open bars show non-significant correlations. Cells with high firing rate variability (SD > 5 imp/s; see Figure 3) are distinguished with dot markers in the histogram. It is evident by inspection that the K cells with high variability are clustered at the left of the histogram, that is, they have high and significant negative correlation with delta power.

In order to further characterise the relation between cortical state and LGN spiking activity, we next used Hilbert analysis to estimate delta band power (see Materials and Methods) and segmented the recording epochs into asynchronous (low-delta) and synchronous (high-delta) states. Across the dataset roughly equal periods of synchronous and asynchronous state were sampled (for low-delta: K, 215 ± 15 s, n = 45; P, 200 ± 16 s, n = 43; M, 153 ± 11 s, n =

25; *Kruskal-Wallis p* = 0.02; for high-delta: K, 163 ± 13 s; P, 163 ± 10 s; M, 173 ± 16 s; *Kruskal-Wallis p* = 0.80). The analysis yields two main results. Firstly, as expected from the data so far, there is a selective link between K cell spike rate fluctuations and cortical state. Figure 5A shows that cells high spike rate variability (SD > 5) were predominantly recorded during asynchronous (low delta) cortical state, and Figure 5B shows that mean spike rate for nearly all of these cells is greater in asynchronous than in synchronous cortical state. Of 19 K cells shown on these plots, 16 (84%) were recorded predominantly in asynchronous cortical state, and 15 (79%) showed higher maintained rate in asynchronous state (chi-square *p* =0.00 for both comparisons). Secondly, and perhaps more surprisingly, the behaviour of K cells is not completely uniform: like P and M cells, some K cells with overall low variability (SD < =5), were predominantly recorded in asynchronous cortical state (Fig. 5C) yet showed no clear link between spike rate and cortical state (two examples are marked with arrows in Fig. 5C, D). These "unlinked" K-cells were not obviously restricted to one region of LGN recordings or one visual response type. Notwithstanding this puzzle, we can conclude that epochs of high spike rate in K cells are predominantly linked to asynchronous cortical state, whereas spike rates of nearly all P and M cells are not influenced by cortical state. The distribution of state times for high and low delta states is shown in Figure 5E, F. Both distributions are heavily skewed to durations below 10 s (low delta mean 5.2 ± 4.4 (n = 3292), high delta mean 6.2 ± 4.1 (n = 1459).

Cortical asynchrony precedes K cell spike rate increases.

An obvious question arising is whether V1 state changes occur before or after K cell spike rate changes. To address this question we used directed Granger causality analysis (Cui et al., 2008). The LFP and spike rates signals were measured in the same way as for the data shown in Figure 4, then both signals were Z-transformed across the 40s recording epoch. Figure 6A shows two examples of low-to-high K cell spike rate transition (thin line) accompanied by high-to-low delta LFP power transition (dotted line). Time is shown relative to the start of the recording epoch.

To enable the Granger analysis we needed to find transitions that were long-lived but did not fall off the borders of the recording epoch. In total 27 clearly defined examples of transitions from low-to-high spike rate (defined as explained in the Materials and Methods section) were identified in 7 K cells. For each transition period, the mean causality in the 0 – 0.5 Hz range was calculated for LGN→V1 and V1→LGN directions. The result is shown as a scatterplot in Figure 6B. Each recorded cell is shown by a different symbol. With one exception, the points lie above or close to the unity line, indicating asynchronous cortical state is a better predictor of LGN spike rate than *vice versa*. Accordingly, the mean V1→LGN causality (1.4 ± 0.12, n = 27) was higher than LGN→V1 causality (0.9 ± 0.09, *Wilcoxon* $p = 0.00$). Analysis of high-to-low spike rate transitions yielded a consistent result (mean V1→LGN causality 1.4 ± 0.6, n=15; LGN→V1 causality 0.9 ± 0.5, *Wilcoxon* $p = 0.00$). These results are broadly consistent with propagation of brain state V1 to LGN, but it is important to remember that the V1 to LGN feedback pathway is part of a complex loop system comprising multiple pathways within and between the LGN, V1, and thalamic reticular nucleus (McCormick, 1989; Contreras and Steriade, 1995; Sherman and Guillery, 1996; Callaway, 2005; Crunelli and Hughes, 2010). We return to the question of causality in a later section, for now we reiterate the main result that changes in cortical state are a better predictor of changes in K cell state than the reverse. For expediency we did not attempt more complex analyses of causality (e.g. Hu et al., 2016).

K cell spike rate fluctuations are independent of spike bursts in LGN

Spike bursts in dorsal thalamic nuclei typically comprise a brief (50-100 ms) pause in spike activity followed by a short train of high-frequency spikes. Spike bursts in thalamus are more common under synchronous (e.g. sleeping) than asynchronous (e.g. waking) cortical states (Contreras and Steriade, 1995; Ramcharan et al., 2000b; reviewed by Sherman and Guillery, 2006). We therefore expected that the frequency of spike bursts in marmoset LGN would be greater in synchronous (high-delta) state than in asynchronous (low-delta) state. Surprisingly

however, we found this not to be the case. We defined bursts using criteria very close to the liberal criteria used by Ramcharan et. al (2000), that is a minimum of 50 ms pause before burst onset and less than 6 ms between burst spikes. Bursts of two spikes are included in the criterion. Plotting interval before spike onset against interval after spike occurrence for a single cell during synchronous (Fig. 7A) and asynchronous (Fig 7B) state shows a very similar pattern. Spikes that are part of a burst are shown as square symbols, all other recorded spikes are shown as black points. In this example during periods of cortical synchrony (Fig. 7A) 101 bursts were detected, while during asynchronous periods (Fig. 7B) 80 bursts were detected. Hilbert phase analysis revealed no selective effect of cortical state on delta phase for burst spikes (Fig. 7C, D).

Overall, K cells show the lowest instance of bursts (0.29 ± 0.4 burst s^{-1}, n = 45), compared to P (0.63 ± 0.6 burst s^{-1}, n = 43) and M cells (0.43 ± 0.3 burst s^{-1}, n = 25, *Kruskal-Wallis p* = 0.00, Figure 7E). Comparison of burst rate during synchronous and asynchronous cortical state (Figure 7F) for any cell population (K cells: 0.29 ± 0.4 *vs*. 0.27 ± 0.3 bursts s^{-1}, n = 45, *paired Wilcoxon p* = 0.95; P cells: 0.63 ± 0.6 *vs.* 0.62 ± 0.5 bursts s^{-1}, n = 43, *p* = 0.5; M cells: 0.45 ± 0.3 *vs.* 0.43 ± 0.3 bursts s^{-1}, n = 25, *p* = 0.88). There was no significant difference in cortical phase of the bursts between cell types (K: -2.0 ± 1.3 rad; M: 2.5 ± 1.3 rad; P: 2.6 ± 1.3 rad, *circular Kruskal-Wallis p* = 0.91). As might be expected from the almost identical appearence of the scatterplots in Figure 7A and Figure 7B, other measures we tested (e.g. burst fraction) and repeat analysis using conservative (100 ms pause, 4 ms between spikes) and very liberal (0 ms pause, 6 ms between spikes) burst criteria, and comparison of K cells showing high (SD > 5) and low (SD <=5) spike rate variability likewise showed negligible differences between synchronous and asynchronous cortical state (data not shown).

These results show that bursts are less frequent in maintained activity of K cells than in maintained activity of M or P cells, and that there is no clear relationship between cortical delta state and LGN cell burst frequency or timing. This conclusion is limited by the fact that (as noted

above in the methods section), our definition of asynchronous state includes more EEG power at sub-gamma frequencies than would be present in studies of waking animals.

K cell spike rate fluctuations interact additively with sensory stimuli

All results described so far are from analysis of on-going (maintained or "spontaneous") activity recorded in absence of patterned visual stimuli. These analyses do not reveal how K cell spike rate fluctuations could interact with, and therefore modulate, sensory signals. Transmission of retinal spikes through LGN is dependent on visual stimulus parameters such as contrast and temporal frequency (Kaplan et al., 1987; Sincich et al., 2007) as well as cortical state (Kaplan et al., 1993; Li et al., 1999; Funke and Eysel, 2000). Specifically, we asked whether the interaction between sensory signal and K cell spike rate fluctuations is additive or multiplicative. Figure 8A shows schematically the predicted effect of additive and multiplicative noise interaction with visually evoked signals. Expressed as a function of noise amplitude, additive noise produces uniform response amplitude increase (change in elevation; left scatterplot) whereas multiplicative noise produces amplitude-dependent increase (change in gain, right scatterplot). Figure 8B shows for a K-bon cell maintained response rate before stimulus (grey square markers, Fig. 8B) and the evoked response rate during stimulus (blue triangle markers, Fig. 8B), across 100 repetitions of a 200 ms S-cone selective pulse. Over the course of ~8 minutes of data collection, the maintained spike rate for this cell varied between 0 and 80 imp s^{-1}. It is immediately obvious that the evoked responses run above and roughly parallel to the maintained responses. Figure 8C shows peristimulus time histograms of evoked responses collected during all trials (left), or trials where maintained spike rate before stimulus onset was high (centre) or low (right). Figure 8D shows a scatter plot of the maintained rate before stimulus onset (x-axis) against the evoked spike rate during stimulus presentation (y-axis) across 126 stimulus presentations. The thick black line shows mean regression ($y = 1.1x + 13$). The slope of the fit is close to the slope of the unity line (thin grey line); thus the evoked visual

response in this K cell is superimposed on a variable baseline, that is, the slow rhythm (see also Figure 4 B–G). Comparable results were obtained for nearly all K cells tested. Figure 9A shows linear fits for individual K cells (thin grey lines) as well as population mean regression ($y = 0.9x + 32$ imp s^{-1}, $n = 20$, thick magenta line). Thus, across our sample, K cells increase their spike rate on average by 32 imp s^{-1} across the 200 ms preferred stimulus presentation, and this increase is independent of spike rate before stimulus onset, indicating additive signal and noise combination.

We next applied receiver operator characteristic (ROC) analysis to cell responses. Technical limitations prevented us from storing V1 LFP signals during these recordings. We therefore used the spike rate before stimulus onset as a proxy for cortical state. This approach is justified because the question we are asking here concerns the relationship of maintained spike rate to stimulus detectability. The analysis does not depend on cortical state *per se*, or make any inference about cortical state. Each stimulus trial was classified as showing low or high spike rate before stimulus onset. A criterion at 20 imp s^{-1} was chosen because 95% of pre-stimulus spike rate samples fell below this value in cells that showed low spike rate variability (SD < 5; 2356 trials recorded from 23 K cells, also *cf.* Fig. 5B, F). The ROC was then calculated for these two spike rate states. Figure 9B shows ROC analysis of the cell shown in Figure 8. We used the area under the curve (AUC) as a measure of stimulus detectability. In this example there is negligible difference in detectability if spike rate before stimulus onset was low (AUC 86%) or high (AUC 83%). The same conclusion can be drawn from the other K cells analysed (Figure 9C, $n = 20$), that is, there is negligible difference in detectability between low or high spike rate before stimulus onset (0.94 ± 0.08 *vs.* 0.91 ± 0.11, *Wilcoxon* $p = 0.10$).

When a cell is presented with an anti-preferred stimulus its spike rate (by definition) decreases. Figure 9D, E shows ROC analysis for an anti-preferred stimulus (S cone contrast decrement) of the cell shown in Figure 8. Here it is apparent that the signal-noise interaction is

better expressed as slope change (multiplicative signal-noise interaction). Consistently, the mean regression slope for anti-preferred stimuli was lower than for preferred stimuli (0.2 ± 0.2 *vs*. 0.9 ± 0.3, paired *Wilcoxon p* =0.00, n = 20). Under high maintained rates the dynamic response range is thus improved (i.e., less rectified) relative to low maintained rates. In consequence, high maintained rates can *improve* the neurometric detectability of anti-preferred stimuli (Figure 9E, AUC 84% for low spike rate; AUC 99% for high spike rates). The same pattern emerges from the population data (Fig. 9F). Trials with high maintained rate before onset (0.97 ± 0.06) are better detectors of evoked spike rate decrements than trials with low spike rate (0.84 ± 0.12, *Wilcoxon p* = 0.00, n=20). We conclude that high spike rates in K cells do not, in principle, degrade the capacity to detect stimuli, and may improve that capacity.

Delta-frequency phase-locking in M, P, and K populations shows cortical state dependence.

The complementary changes in cortical state and K cell spike rate described above take place across multi-second timescales. We previously showed that synchronous activity in pairs and ensembles of K cells can also be detected at sub-second timescales (Cheong et al., 2011). Therefore we asked if LFP delta band activity is linked to spike rates at the sub-second timescale of individual delta-band waves (1–4 Hz). Figure 10A shows raw V1 local field potential trace (black, upper), delta band filtered trace (blue, centre), and simultaneously recorded spikes from a single K cell (blue triangles, lower). We used Hilbert transform to calculate the instantaneous phase of the delta band signal for each spike across the 40s recording epochs for K cells (n=45), M cells (n=25) and P cells (n=43). Cortical state was classified as asynchronous (low delta power) or synchronous (high delta power) as described in the Materials and Methods section. Figure 10B shows an example phase distribution for spikes of a single K-bon cell during a total 176 s recording made during high-delta state. We used Rayleigh's non-uniformity test to estimate the strength of phase locking of spikes to delta waves. In this example the spike

probability is highest slightly before the delta wave peak (mean angle ± variance, -1.44 ± 0.9 rad, vector length = 0.1, *Rayleigh's test for non-uniformity p* =0.00,).

Across all LGN cell types, we found about 50% of each population (K: 22/45, M: 14/25, P: 22/43) shows significant phase locking during high-delta state (Figure 10C). Figure 10D is a vector plot of preferred phase angle and bias strength for the ~50% of cells showing phase locking in high-delta state (thin lines) and mean (thick line) vector (mean angle ± variance, K cells: -2.36 ± 0.6 rad, vector length = 0.4; M cells: 2.72 ± 0.39 rad, vector length = 0.61; P cells: -2.97 ± 0.55 rad, vector length = 0.45). Spiking in most LGN cells is phase biased around the trough of V1 delta waves. During asynchronous cortical state, for K and P cells the angle of phase locking remained similar, but the mean angle for M cells moved closer to the peak of V1 delta waves (mean angle ± variance, K cells: -2.09 ± 0.43 rad, vector length = 0.57; M cells: -0.36 ± 0.87 rad, vector length = 0.13; P cells: 2.84 ± 0.44 rad, vector length = 0.56).

The proportion of phase locked cells decreases to ~25% for all LGN populations under asynchronous cortical state (K cells: 11/45, M cells: 8/25, P cells: 8/43, Fig. 10C). This last result shows that whereas only K cell spike rates are linked to slow changes in cortical state, delta-band thalamocortical synchrony is lower in all LGN divisions under asynchronous cortical state than under synchronous cortical state.

Discussion.

We found that in synchronous cortical state, activity throughout all (P, M, and K) divisions of the LGN is entrained to delta-band cortical oscillations. Switches from synchronous to asynchronous state are accompanied by spike rate changes in K pathway cells, and by decreased delta entrainment in all LGN divisions. The switches from synchronous to asynchronous cortical state precede (normally by 1 – 3s) the switches from low to high K cell spike rate, implying that asynchronous cortical state could be the cause of spike rate changes in the K layers.

Furthermore, switches in K cell spike rates do necessarily not come at cost of faithful visually-evoked signal transmission.

We found uniform phase-locking to delta waves across the LGN under synchronous cortical state. Entrainment of thalamic and cortical activity is consistently observed across species and dorsal thalamic nuclei studied so far in non-primate mammals (Contreras and Steriade, 1995; Rigas and Castro-Alamancos, 2007; Crunelli and Hughes, 2010; and references therein), and we show here (to our knowledge for the first time) a consistent pattern of delta-band entrainment in primate LGN. We concentrated on delta-band cortical activity, but LGN coherence to other temporal frequency bands should likely show a similar pattern (Lőrincz et al., 2009). Thalamocortical coherence at low frequencies has been specifically linked to low threshold calcium channels and thalamic burst activity (Steriade et al., 1993; von Krosigk et al., 1993; Ramcharan et al., 2000a; Llinás and Steriade, 2006; Crunelli and Hughes, 2010). In our experiments however we did not see a clear relation between LGN burst activity and the phase of delta-frequency oscillations (Fig. 7), and we found overall little burst activity in marmoset LGN.

Ramcharan et al. (Ramcharan et al., 2000a) found overall low frequency of bursts in waking macaque LGN, on comparison to somatosensory thalamus. They suggest that relatively high levels of synaptic bombardment from retinal inputs could serve to keep LGN cells in a more depolarised state than relay cells in other dorsal thalamic nuclei. On the other hand, Livingstone and Hubel (Livingstone and Hubel, 1981) showed increased burst activity associated with delta-band EEG activity in LGN of cats in transition from waking to sleeping state (see also Funke and Eysel, 2000; Kaplan et al., 1987). Thus in addition to differences between thalamic nuclei there may be differences between carnivores and primates in the relation of LGN bursting and cortical state.

We found selective covariance of K cell activity with cortical state, whereby asynchronous cortical states are linked to high spike rates in K cells. These results are obtained from a much larger sample of LGN cells (60 K cells, 43 P cells, 25 M cells) than the results of Cheong et al (2011), who measured total 27 LGN cells. In addition, our Granger causality analysis (Figure 6A, B) suggests that slow changes in brain state propagate from V1 to K cells in LGN. If this link is causal, then the asynchronous cortical state is promoting increased spike rates in part of the afferent thalamic input streams. On the other hand, Tan et al. (2014) showed that increased spike rates in thalamic inputs can cause the cortex to shift from synchronous to asynchronous state. We speculate that two processes act as a positive feedback circuit, whereby loss of synchrony in the cortex raises K cell spike rate, which in turn leads to further cortical desynchronisation. In this way, the K pathway could be viewed as part of a circuit controlling switches between synchronous and asynchronous cortical states. Of course, our observations are made under anaesthesia, so the extent to which these physiological principles would apply to conscious visual processing is not yet known.

In addition to showing widespread terminations in supragranular layers of V1 (Blasdel and Lund, 1983; Fitzpatrick et al., 1983; Casagrande et al., 2007), K pathways are distinct to P and M pathways in providing inputs to non-striate cortical visual areas (Bullier and Kennedy, 1983; Sincich et al., 2004; Warner et al., 2010). These anatomical features have led to the *thalamocortical synchrony* hypothesis (Jones, 2001; Jones, 2009) whereby cortical activity generated by K pathways could coordinate activity within and between visual cortical area and generate coherent thalamo-cortical oscillations. Our cortical recordings were limited to V1, and we do not have direct evidence that K pathway is involved in controlling cortical state. Our results are nevertheless consistent with the thalamocortical synchrony hypothesis, because they show that slow cortical state changes are more tightly linked to by K pathway activity than to P and M pathway activity.

Mechanisms

There is anatomical (Lund et al., 1975; Fitzpatrick et al., 1994; Usrey and Fitzpatrick, 1996) and physiological evidence (Briggs and Usrey, 2007; Briggs and Usrey, 2009) for parallel organization of cortico-geniculate pathways. Thus there are anatomical bases for selective propagation of cortical state to K cells but not P or M cells. Further, there is anatomical and physiological evidence for merger of K, P, and M afferent pathways at early stages of cortical processing (Yoshioka et al., 1994; Cottaris and DeValois, 1998; Vidyasagar et al., 2002; Callaway, 2005). In this way activated K cells and intrinsic cortical circuitry (Fröhlich et al., 2006) could support asynchronous cortical activity. This scenario does not rule out a role of the connections of K layers to subcortical centres regulating eye movements, vigilance, and attention (Harting et al., 1978; Casagrande, 1994; Bickford et al., 2000). For example, the basal nucleus of Meynert has widespread diffuse cholinergic connections with cortex as well as thalamus, and could initiate or propagate changes in cortical state (reviewed by Semba, 2000; Steriade, 2004).

Summary

The traditional view of the LGN as a relay structure has given way to the modern view of the LGN as one participant in a group of thalamo-cortico-thalamic loops that serve perception and cognition (Jones, 2001; Sherman and Guillery, 2006; Steriade, 2006). Here we show that low-frequency changes in K cell reflect changes in thalamocortical coherence across the LGN. It is known that sensory signals at the LGN level can be influenced by attention processes (O'Connor et al., 2002; McAlonan et al., 2008; Saalmann and Kastner, 2011; Jiang et al., 2015). Thus a change in brain state and loss of phase locking between LGN cells and cortex could indicate a first step in modulating sensory information in all LGN layers. It would obviously be of interest to know if what we find here for anaesthetised marmosets also applies to behavioural state transitions in awake animals.

References

Berens P (2009). CircStat: A Matlab toolbox for circular statistics. *Journal of Statistical Software* **31**,

Bickford ME, Ramcharan E, Godwin DW, Erişir A, Gnadt J & Sherman SM (2000). Neurotransmitters contained in the subcortical extraretinal inputs to the monkey lateral geniculate nucleus. *J Comp Neurol* **424**, 701-717.

Blasdel GG & Lund JS (1983). Termination of afferent axons in macaque striate cortex. *J Neurosci* **3**, 1389-1413.

Blessing EM, Solomon SG, Hashemi-Nezhad M, Morris BJ & Martin PR (2004). Chromatic and spatial properties of parvocellular cells in the lateral geniculate nucleus of the marmoset (*Callithrix jacchus)*. *J Physiol* **557**, 229-245.

Bokil H, Andrews P, Kulkarni JE, Mehta S & Mitra PP (2010). Chronux: a platform for analyzing neural signals. *J Neurosci Methods* **192**, 146-151.

Bradley AP (1997). The use of the area under the ROC curve in the evaluation of machine learning algorithms. *Pattern Recognit* **30**, 1145-1159.

Briggs F & Usrey WM (2007). A fast, reciprocal pathway between the lateral geniculate nucleus and visual cortex in the macaque monkey. *J Neurosci* **27**, 5431-5436.

Briggs F & Usrey WM (2009). Parallel processing in the corticogeniculate pathway of the macaque monkey. *Neuron* **62**, 135-146.

Bullier J & Kennedy H (1983). Projection of the lateral geniculate nucleus onto cortical area V2 in the macaque monkey. *Exp Brain Res* **53**, 168-172.

Buzás P, Blessing EM, Szmajda BA & Martin PR (2006). Specificity of M and L cone inputs to receptive fields in the parvocellular pathway: random wiring with functional bias. *J Neurosci* **26**, 11148-11161.

Buzsáki G & Draguhn A (2004). Neuronal oscillations in cortical networks. *Science* **304**, 1926-1929.

Callaway EM (2005). Neural substrates within primary visual cortex for interactions between parallel visual pathways. *Prog Brain Res* **149**, 59-64.

Casagrande V, Yazar F, Jones K & Ding Y (2007). The morphology of the koniocellular axon pathway in the macaque monkey. *Cereb Cortex* **17**, 2334-2345.

Casagrande VA (1994). A third parallel visual pathway to primate area V1. *Trends Neurosci* **17**, 305-310.

Cheong SK & Pietersen AN (2014). Antidromic latency of magnocellular, parvocellular, and koniocellular (Blue-ON) geniculocortical relay cells in marmosets. *Visual Neurosci* **31**, 263-273.

Cheong SK, Tailby C, Martin PR, Levitt JB & Solomon SG (2011). Slow intrinsic rhythm in the koniocellular visual pathway. *Proc Natl Acad Sci USA* **108**, 14659-14663.

Cheong SK, Tailby C, Solomon SG & Martin PR (2013). Cortical-Like Receptive Fields in the Lateral Geniculate Nucleus of Marmoset Monkeys. *J Neurosci* **33**, 6864-6876.

Contreras D & Steriade M (1995). Cellular basis of EEG slow rhythms: a study of dynamic corticothalamic relationships. *J Neurosci* **15**, 604-622.

Cottaris NP & DeValois RL (1998). Temporal dynamics of chromatic tuning in macaque primary visual cortex. *Nature* **395**, 896-900.

Crunelli V & Hughes SW (2010). The slow (<1 Hz) rhythm of non-REM sleep: a dialogue between three cardinal oscillators. *Nat Neurosci* **13**, 9-17.

Cui J, Xu L, Bressler SL, Ding M & Liang H (2008). BSMART: a Matlab/C toolbox for analysis of multichannel neural time series. *Neural Netw* **21**, 1094-1104.

Destexhe A, Contreras D & Steriade M (1998). Mechanisms underlying the synchronizing action of corticothalamic feedback through inhibition of thalamic relay cells. *J Neurophysiol* **79**, 999-1016.

Dreher B, Fukada Y & Rodieck RW (1976). Identification, classification and anatomical segregation of cells with X-like and Y-like properties in the lateral geniculate nucleus of Old-World primates. *J Physiol* **258**, 433-452.

Fitzpatrick D, Itoh K & Diamond IT (1983). The laminar organization of the lateral geniculate body and the striate cortex in the squirrel monkey (*Saimiri sciureus*). *J Neurosci* **3**, 673-702.

Fitzpatrick D, Usrey WM, Schofield BR & Einstein G (1994). The sublaminar organization of corticogeniculate neurons in layer 6 of macaque striate cortex. *Visual Neurosci* **11**, 307-315.

Forte JD, Blessing EM, Buzás P & Martin PR (2006). Contribution of chromatic aberrations to color signals in the primate visual system. *J Vision* **6**, 97-105.

Fröhlich F, Bazhenov M, Timofeev I, Steriade M & Sejnowski TJ (2006). Slow state transitions of sustained neural oscillations by activity-dependent modulation of intrinsic excitability. *J Neurosci* **26**, 6153-6162.

Funke K & Eysel UT (2000). Quantitative aspects of the state-dependent co-variation of cat

lateral geniculate and perigeniculate visual activity. *Neuroreport*

Grundy D (2015). Principles and standards for reporting animal experiments in The Journal of Physiology and Experimental Physiology. *Experimental physiology* **100**, 755-758.

Harting JK, Casagrande VA & Weber JT (1978). The projection of the primate superior colliculus upon the dorsal lateral geniculate nucleus: autoradiographic demonstration of interlaminar distribution of tectogeniculate axons. *Brain Res* **150**, 593-599.

Hendry SHC & Reid RC (2000). The koniocellular pathway in primate vision. *Ann Rev Neurosci* **23**, 127-153.

Hu M, Li M, Li W & Liang H (2016). Joint analysis of spikes and local field potentials using copula. *Neuroimage* **133**, 457-467.

Jiang Y, Yampolsky D, Purushothaman G & Casagrande VA (2015). Perceptual decision related activity in the lateral geniculate nucleus. *J Neurophysiol* **114**, 717-735.

Jones EG (2001). The thalamic matrix and thalamocortical synchrony. *Trends Neurosci* **24**, 595-601.

Jones EG (2007). *The Thalamus (2nd edition)*. Cambridge University Press, Cambridge.

Jones EG (2009). Synchrony in the interconnected circuitry of the thalamus and cerebral cortex. *Ann NY Acad Sci* **1157**, 10-23.

Kaplan E & Benardete E (2001). The dynamics of primate retinal ganglion cells. *Prog Brain Res* **134**, 17-34.

Kaplan E, Mukherjee P & Shapley R (1993). Information filtering in the lateral geniculate nucleus. In *Contrast Sensitivity*, ed. R.Shapley & Lam D-K. pp. 183-200. The MIT Press,

Cambridge.

Kaplan E, Purpura K & Shapley RM (1987). Contrast affects the transmission of visual information through the mammalian lateral geniculate nucleus. *J Physiol* **391**, 267-288.

Kaplan E & Shapley RM (1986). The primate retina contains two types of ganglion cells, with high and low contrast sensitivity. *Proc Natl Acad Sci USA* **83**, 2755-2757.

Le Van Quyen M, Foucher J, Lachaux J, Rodriguez E, Lutz A, Martinerie J & Varela F (2001). Comparison of Hilbert transform and wavelet methods for the analysis of neuronal synchrony. *J Neurosci Methods* **111**, 83-98.

Li B, Funke K, Wörgötter F & Eysel UT (1999). Correlated variations in EEG pattern and visual responsiveness of cat lateral geniculate relay cells. *J Physiol* **514**, 857-874.

Livingstone MS & Hubel DH (1981). Effects of sleep and arousal on the processing of visual information in the cat. *Nature (London)* **291**, 554-561.

Llinás RR & Steriade M (2006). Bursting of thalamic neurons and states of vigilance. *J Neurophysiol* **95**, 3297-3308.

Lőrincz ML, Kékesi KA, Juhász G, Crunelli V & Hughes SW (2009). Temporal framing of thalamic relay-mode firing by phasic inhibition during the alpha rhythm. *Neuron* **63**, 683-696.

Lund JS, Lund RD, Hendrickson AE, Bunt AH & Fuchs AF (1975). The origin of efferent pathways from the primary visual cortex, area 17, of the macaque monkey as shown by retrograde transport of horseradish peroxidase. *J Comp Neurol* **164**, 287-303.

Martin PR, White AJR, Goodchild AK, Wilder HD & Sefton AE (1997). Evidence that blue-on cells are part of the third geniculocortical pathway in primates. *Eur J Neurosci* **9**, 1536-1541.

McAlonan K, Cavanaugh J & Wurtz RH (2008). Guarding the gateway to cortex with attention in visual thalamus. *Nature* **456**, 391-394.

McCormick DA (1989). Cholinergic and noradrenergic modulation of thalamocortical processing. *Trends Neurosci* **12**, 215-221.

McCormick DA, Bal T & VonKrosigk M (1992). Cellular basis and neurotransmitter control of thalamic oscillation and sensory transmission. In *Thalamic Networks for Relay and Modulation*, ed. Minciacchi D, Molinari, M., Macchi, G. & Jones, E.G. pp. 357-373. Pergamon Press, Oxford.

Nassi JJ & Callaway EM (2009). Parallel processing strategies of the primate visual system. *Nat Rev Neurosci* **10**, 360-372.

O'Connor DH, Fukui MM, Pinsk MA & Kastner S (2002). Attention modulates responses in the human lateral geniculate nucleus. *Nat Neurosci* **5**, 1203-1209.

Pietersen AN, Cheong SK, Solomon SG, Tailby C & Martin PR (2014). Temporal response properties of koniocellular (blue-on and blue-off) cells in marmoset lateral geniculate nucleus. *J Neurophysiol* **112**, 1421-1438.

Ramcharan EJ, Cox CL, Zhan XJ, Sherman SM & Gnadt JW (2000a). Cellular mechanisms underlying activity patterns in the monkey thalamus during visual behavior. *J Neurophysiol* **84**, 1982-1987.

Ramcharan EJ, Gnadt JW & Sherman SM (2000b). Burst and tonic firing in thalamic cells of unanesthetized, behaving monkeys. *Visual Neurosci* **17**, 55-62.

Rigas P & Castro-Alamancos MA (2007). Thalamocortical Up states: differential effects of intrinsic and extrinsic cortical inputs on persistent activity. *J Neurosci* **27**, 4261-4272.

Roy S, Martin PR, Dreher B, Saalmann YB, Hu D & Vidyasagar (2009). Segregation of short-wavelength sensitive (S) cone signals in the macaque dorsal lateral geniculate nucleus. *Eur J Neurosci* **30**, 1517-1526.

Saalmann YB & Kastner S (2011). Cognitive and perceptual functions of the visual thalamus. *Neuron* **71**, 209-223.

Semba K (2000). Multiple output pathways of the basal forebrain: organization, chemical heterogeneity, and roles in vigilance. *Behav Brain Res* **115**, 117-141.

Sherman SM (2016). Thalamus plays a central role in ongoing cortical functioning. *Nat Neurosci* **16**, 533-541.

Sherman SM & Guillery RW (1996). Functional organization of thalamocortical relays. *J Neurophysiol* **76**, 1367-1395.

Sherman SM & Guillery RW (2006). *Exploring the thalamus and its role in cortical function*. MIT press, Cambridge.

Sincich LC, Adams DL, Economides JR & Horton JC (2007). Transmission of spike trains at the retinogeniculate synapse. *J Neurosci* **27**, 2683-2692.

Sincich LC, Park KF, Wohlgemuth MJ & Horton JC (2004). Bypassing V1: a direct geniculate input to area MT. *Nat Neurosci* **7**, 1123-1128.

Steriade M (2003). *Neuronal substrates of sleep and epilepsy*. Cambridge University Press, Cambridge.

Steriade M (2004). Acetylcholine systems and rhythmic activities during the waking--sleep cycle. *Prog Brain Res* **145**, 179-196.

Steriade M (2006). Grouping of brain rhythms in corticothalamic systems. *Neuroscience* **137**, 1087-1106.

Steriade M, McCormick DA & Sejnowski TJ (1993). Thalamocortical oscillations in the sleeping and aroused brain. *Science* **262**, 679-685.

Szmajda BA, Buzás P, FitzGibbon T & Martin PR (2006). Geniculocortical relay of blue-off signals in the primate visual system. *Proc Natl Acad Sci USA* **103**, 19512-19517.

Szmajda BA, Martin PR & Grünert U (2008). Retinal ganglion cell inputs to the koniocellular pathway. *J Comp Neurol* **510**, 251-268.

Tailby C, Solomon SG, Dhruv NT, Majaj NJ, Sokol SH & Lennie P (2007). A new code for contrast in the primate visual pathway. *J Neurosci* **27**, 3904-3909.

Tailby C, Szmajda BA, Buzás P, Lee BB & Martin PR (2008). Transmission of blue (S) cone signals through the primate lateral geniculate nucleus. *J Physiol* **586**, 5947-5967.

Tan AY, Chen Y, Scholl B, Seidemann E & Priebe NJ (2014). Sensory stimulation shifts visual cortex from synchronous to asynchronous states. *Nature* **509**, 226-229.

Usrey WM & Fitzpatrick D (1996). Specificity in the axonal connections of layer VI neurons in tree shrew striate cortex: evidence for distinct granular and supragranular systems. *J Neurosci* **16**, 1203-1218.

Vidyasagar TR, Kulikowski JJ, Lipnicki DM & Dreher B (2002). Convergence of parvocellular and magnocellular information channels in the primary visual cortex of the macaque. *Eur J Neurosci* **16**, 945-956.

von Krosigk M, Bal T & McCormick DA (1993). Cellular mechanisms of a synchronized oscillation in the thalamus. *Science* **261**, 361-364.

Wang XJ (2010). Neurophysiological and computational principles of cortical rhythms in cognition. *Physiol Rev* **90**, 1195-1268.

Warner CE, Goldshmit Y & Bourne JA (2010). Retinal afferents synapse with relay cells targeting the middle temporal area in the pulvinar and lateral geniculate nuclei. *Front Neuroanat* **4**, 8/1 - 8/16.

White AJR, Goodchild AK, Wilder HD, Sefton AE & Martin PR (1998). Segregation of receptive field properties in the lateral geniculate nucleus of a New-World monkey, the marmoset *Callithrix jacchus. J Neurophysiol* **80**, 2063-2076.

White AJR, Solomon SG & Martin PR (2001). Spatial properties of koniocellular cells in the lateral geniculate nucleus of the marmoset *Callithrix jacchus*. *J Physiol* **533**, 519-535.

Wiesel TN & Hubel D (1966). Spatial and chromatic interactions in the lateral geniculate body of the rhesus monkey. *J Neurophysiol* **29**, 1115-1156.

Yoshioka T, Levitt JB & Lund JS (1994). Independence and merger of thalamocortical channels within macaque monkey primary visual cortex: Anatomy of interlaminar projections. *Visual Neurosci* **11**, 467-489.

Zagha E & McCormick DA (2014). Neural control of brain state. *Curr Opin Neurobiol* **29**, 178-186.

Conflicts of interest: No conflicts of interest, financial or otherwise, are declared by the author(s).

Author contributions

A.N.J.P, S.C., P.R.M., and S.G.S. designed research; A.N.J.P, S.C., P.R.M., and S.G.S. performed research; A.N.J.P, S.C., B.M., P.G, P.R.M and S.G.S. analysed data; A.N.J.P. and P.R.M drafted the

paper; all authors revised the paper critically for important intellectual content. All authors approved submission of this version.

Funding

Australian National Health and Medical Research Council Grants 1027913 and 1005427, Australian Research Council grants CE140100007 and DP160104316.

Acknowledgements

We thank A. Demir and C. Guy for technical assistance, S.S. Solomon (no relation to S.G. Solomon), S. Chen and N. Zeater for assistance with data collection, and R. Townsend for assistance with data analysis.

Figure legends

Figure 1. Illustration showing alternative scenarios for organization of reciprocal circuits between lateral geniculate nucleus (LGN) and primary visual cortex (V1). Many connections (e.g. with thalamic reticular nucleus) are omitted for clarity. A, Parallel reciprocal pathways connect parvocellular (P), koniocellular (K) and magnocellular (M) layers of the LGN to distinct non-interacting circuits in V1. B, Parallel afferent pathways engage with linked cortical circuits enabling functional interaction between P, K, and M pathways at cortical level, and in thalamocortical pathways to LGN. For simplicity the K projections to different cortical layers are not distinguished in this figure.

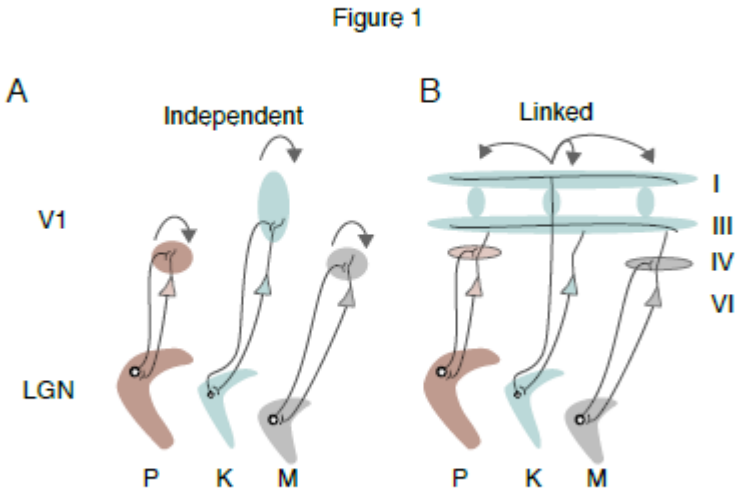

Figure 2. A, Response profile of the most commonly recorded koniocellular cell type, the cone opponent 'Blue-ON' (K-bon) cell. Visual field eccentricity 5.5 deg. Left, peristimulus time histograms (PSTH) of responses to 200 ms square wave pulse stimuli: achromatic increment (ACH+), short-wave cone-isolating increment (S+) and medium/long-wave cone-isolating increment (ML+). Stimulus duration is shown beneath each PSTH. Right, spatial frequency tuning for S cone-isolating drifting gratings. B, Responses of a magnocellular on-centre cell (M-on) in same format as panel (A). Visual field eccentricity 6.7 deg. Tuning curve shows responses to achromatic gratings. Inset panel shows contrast-response function for optimum spatial frequency gratings. *C*, Response of a parvocellular off-centre cell (P-off) in same format as panel (B). Visual field eccentricity 6.9 deg. PSTHs show response to decrement pulses. *D*, Simultaneous recording of local field potential (LFP) in V1 and spike rate of the K cell shown in (A). The black trace (upper) shows unfiltered LFP, the blue trace (center) is LFP band-pass filtered for delta frequencies (1–4 Hz). Tick marks on the lower panel show individual K cell action potentials, the grey bars show the PSTH. Note the increase in spike rate during periods of

cortical asynchrony (low delta power). E, Responses of the M cell in the same format as panel (D). *F*, responses of the P cell in same format as panel (D).

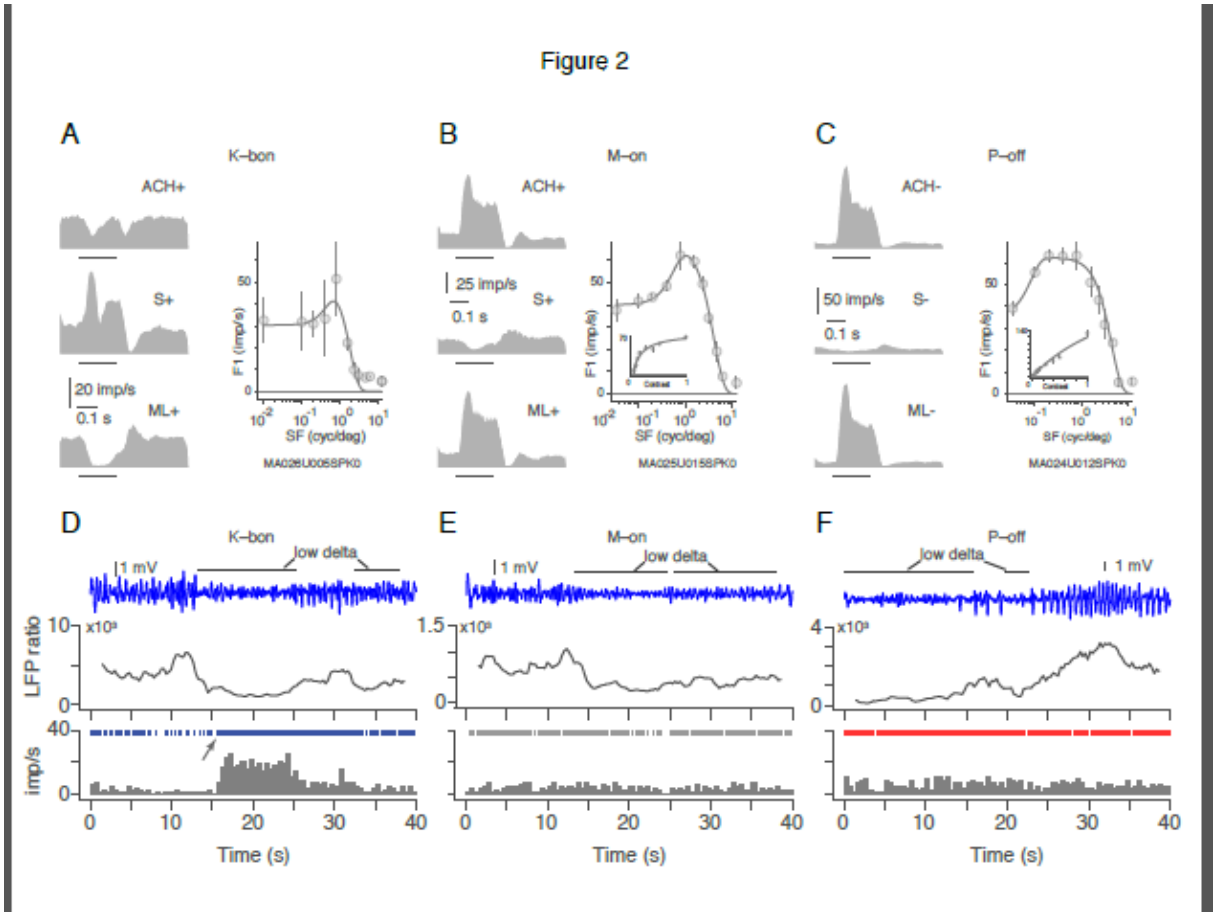

Figure 3. ***A***, Average maintained spike rates across koniocellular (K), magnocellular (M), and parvocellular (P) cell populations. Each point shows average for one cell across 480–720 s recording. Grey bars show mean and standard deviation (SD) for each population. Average spike rate is not significantly different across the populations. *B*, Histogram of variability in spike rate of K cells. About half of the K cells show SD greater than 5 imp s^{-1} *C*, Four M cells show SD greater than 5 imp s^{-1}. *D*, Three P cells show SD greater than 5 imp s^{-1}.

Figure 3

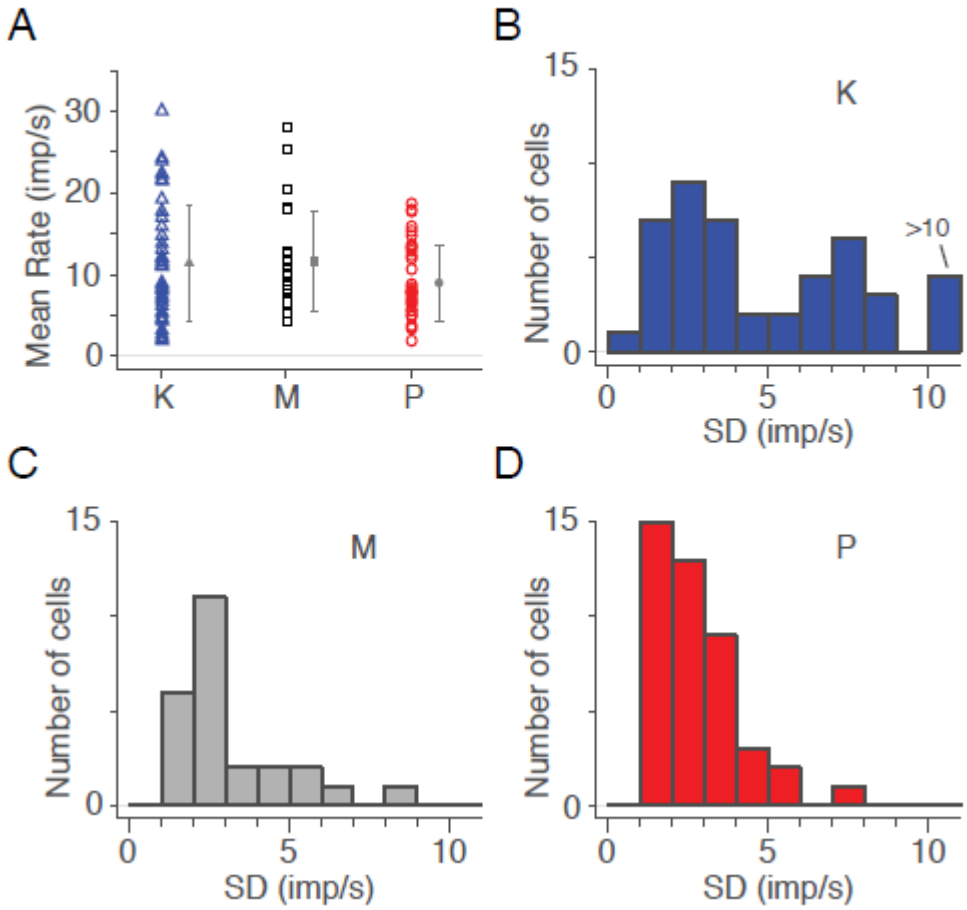

Figure 4. A, Moving window (3 seconds, 0.3 second steps) spectrogram of local field potential (LFP) in V1 (upper), K cell spike rate (center), and average power in LFP frequency bands (bottom) of a 40s recording epoch (this cell is also shown in Figure 2A and 2D). In the spectrogram warm colours indicate higher power. The LFP was normalized to the mean power at 80–100 Hz. Note the loss of warm colours in the lower frequencies between 10–15 seconds, shortly before an increase in K cell spike rate. B–E, Four examples of the relationship between LGN cell spike rate (x-axis) and relative delta-band LFP power (y-axis). All cells have spike rate

variability greater than 5 imp s^{-1} (see Figure 1D). Each circle represents one windowed sample calculated as in (A). Both K cells (B and C) show a negative correlation between spike rate and LFP ratio, whereas the M and P cells (D and E respectively) show no clear relationship. F–G, ccorrelation coefficients derived from linear regression of LGN cell spike rate and delta LFP ratio. Grey bars show cells with a significant correlation; open bars show non-significant correlations. Cells with high firing rate variability (SD > 5 imp/s; see Figure 3) are distinguished with dot markers in the histogram. Note that K cells with high variability cluster to the left of the histogram, indicating high negative correlation.

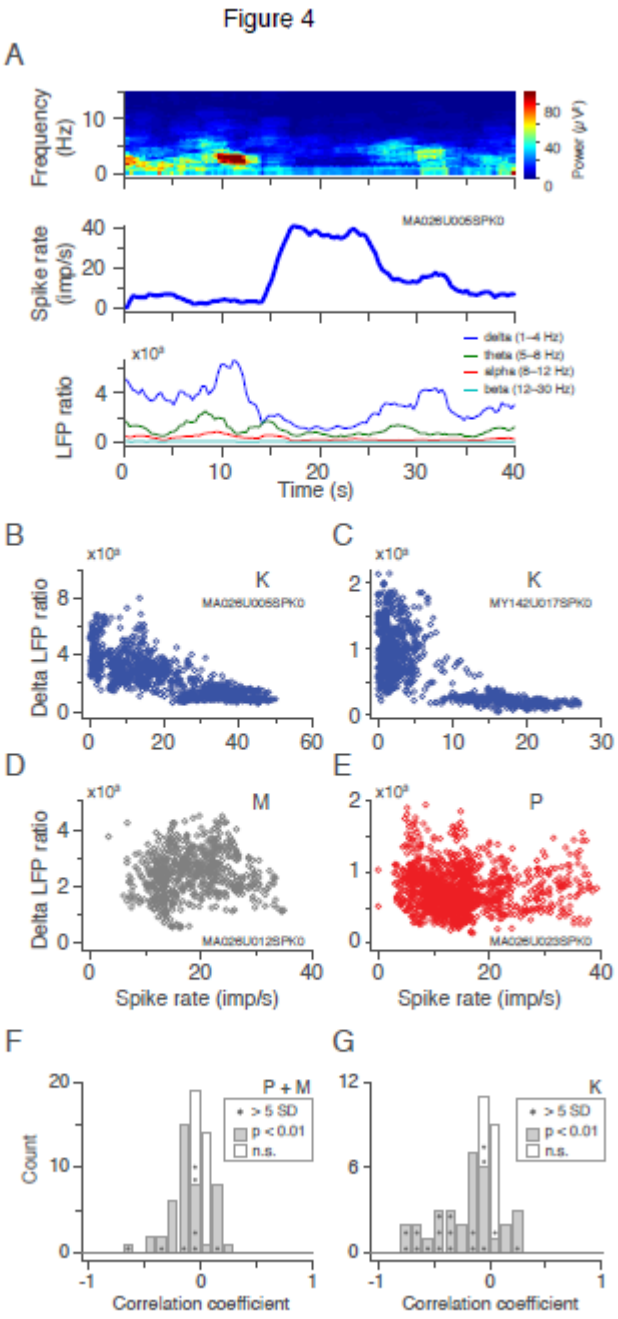

Figure 5. Comparison of cells showing high and low variance in maintained activity. A, scatterplot, for high variance cells, of the cumulated recording time where cortex was in synchronous (high delta) or asynchronous (low delta) state. B, comparison, for high variance cells, of mean discharge rate in high delta and low delta state. Note that nearly all K cells show

increased spike rate in asynchronous cortical state. C, comparison of cells showing low variance, in same format as panel A. Arrows mark examples of K cells recorded predominantly in asynchronous cortical state. D, comparison of spike rates, in same format as panel B. Note that spike rates of the marked K cells show negligible change. E, histogram of high delta state durations. F, histogram of low delta state durations.

Figure 5

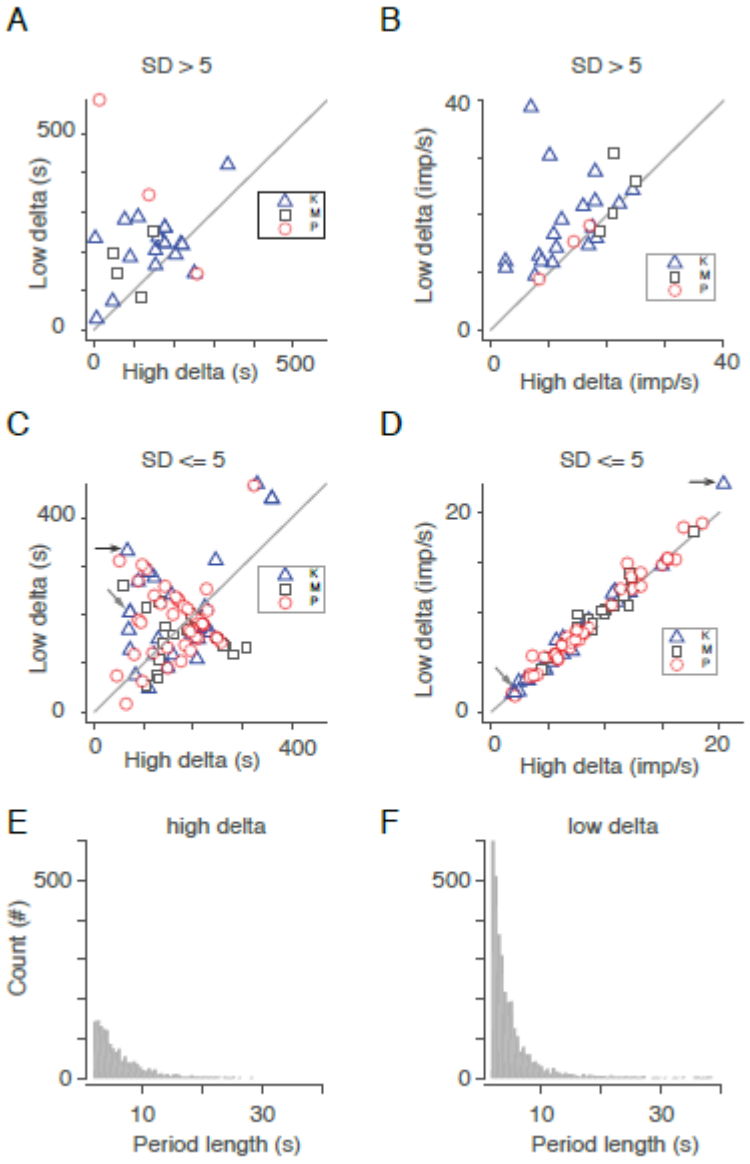

Figure 6. *A*, Two examples of a cortical state change. Thick grey line shows maintained spike rate of a single K cell, broken line shows local field potential (LFP) delta-band power ratio. Data are z-scored to allow direct comparison. Time on the x-axis is the relative time from the start of the 40 s recording epoch. *B*, Granger causality of 27 transitions recorded in 7 K cells. Each symbol indicates a different K cell. The black line is the unity line. The x-axis is mean directed causality LGN to V1 over the transition period; the y-axis is the mean directed V1 to LGN. On average most transitions fall above the unity line indicating V1 state predicts K cell spike rates.

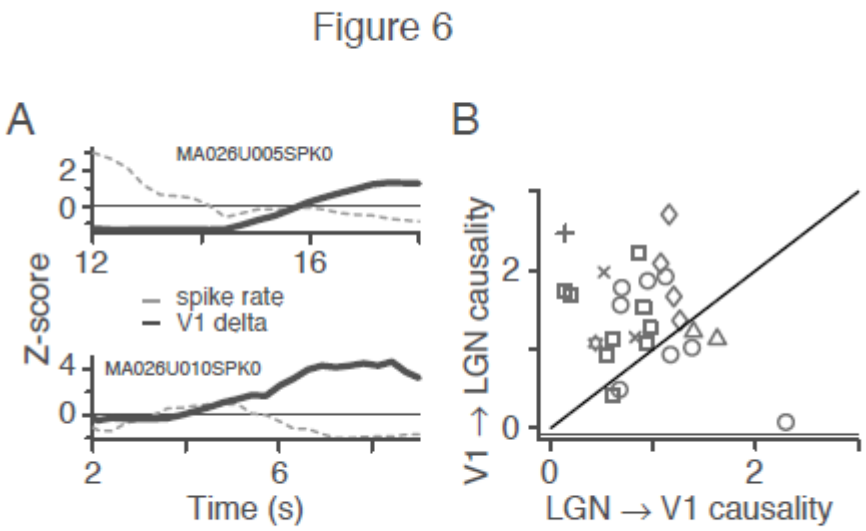

Figure 7. ***A***, Scatterplot of inter-spike interval (ISI) during synchronous (high delta) cortical state. Square symbols show spikes that were classified as part of a burst. Black dots show non-burst spikes. Solid grey lines show thresh- old ISIs of spikes within the burst (6 ms). Broken grey lines show threshold before-spike interval (50 ms). *B*, ISI scatterplot of the same cell during asynchronous (low delta) state. No clear difference to synchronous state is evident. *C–D*, Delta phase of the burst during synchronous (high delta, C) and asynchronous (low delta, D)

cortical periods. There is no preferred phase where bursts occur. *E*, Number of bursts per second for K, P and M cells. Significantly fewer bursts were recorded in K cells ($p < 0.02$,). *F*, No difference was recorded between the instance of bursts during synchronous (high delta) and asynchronous (low delta) cortical periods for K, P or M cells.

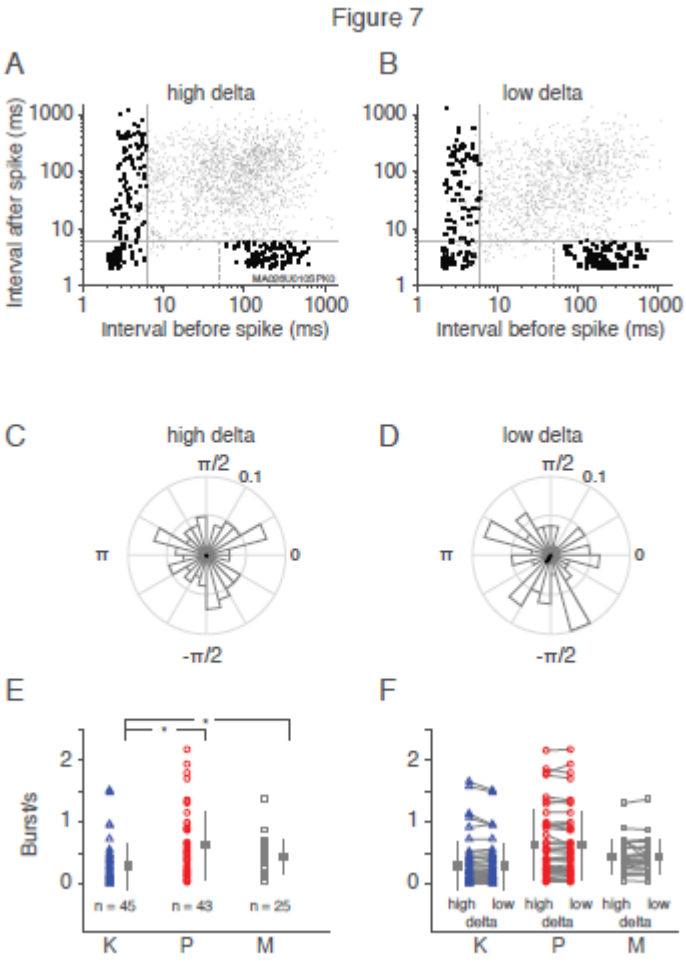

Figure 8. *A*, Predicted effects of signal interaction under additive or multiplicative noise. Additive noise (left) predicts a uniform increase in signal + noise response amplitude (blue points on scatterplot). Multiplicative noise (right) predicts amplitude-dependent increase in signal × noise. *B*, Evoked response amplitude of a K-bon cell before (grey) and during (blue)

repeated presentations to a 200 ms S cone pulse. *C*, peristimulus time histograms of all stimuli (left) and during periods of high (center) and low (right) maintained activity. Dark bar indicates stimulus duration, which was also the spike rate measurement window. *D*, Same data as in panel (*B*) but expressed as mean spike rate in 350 ms before stimulus onset (x-axis) against mean spike rate during the 200 ms stimulus. Stimulus is a S cone isolating increment (S-ON). Open and filled points respectively show stimulus presentations where spike rate before stimulus onset was below or above 20 imp/s. Black line shows the linear regression through all points, formula on the bottom right. Grey line is the unity line.

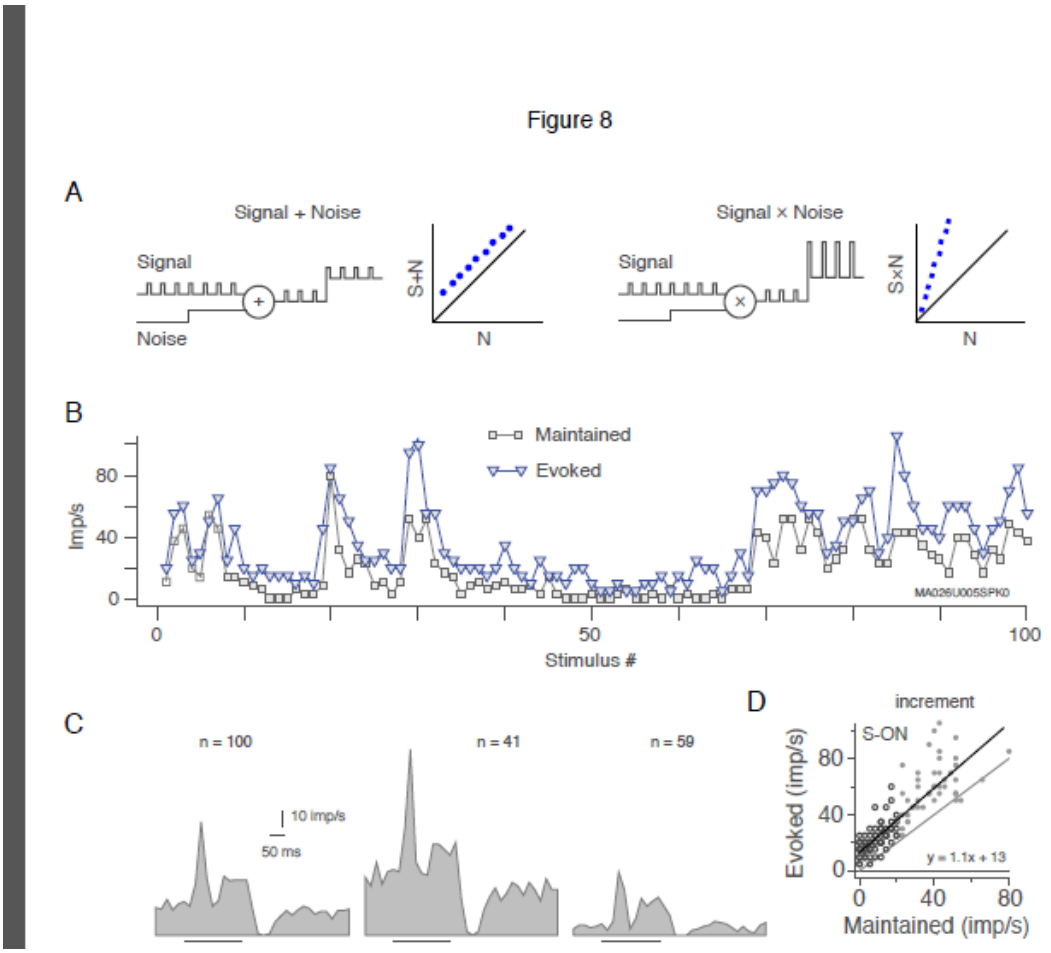

Figure 9. Receiver operating curve (ROC) analysis. *A*, Linear regression of K cell responses to preferred stimulus polarity, calculated as illustrated in Figure 8 D. Grey lines show individual K

cells, magenta thick line shows mean regression line, back line shows unity line. The formula on the bottom right is the formula from the mean regression. *B*, Performance curves from Receiver Operator Characteristic (ROC) analysis from the same data as in (*8A*). The light broken line is the performance from points with high spike rate before stimulus onset, the thin solid line is the performance of points with low spike rate before stimulus onset. The number in the legend is area under the curve expressed as percentage. *C*, ROC analysis for all K blue on cells (n = 20) to S cone increments. Triangles and squares represent individual cells (square = 'blue-OFF', triangle = 'blue-ON'). Grey squares show the mean ± SEM. *D*, Response of the same cell as in Figure 8, but for S-cone isolating decrement (S-OFF) stimulus. *E*, Performance curves from ROC analysis for responses to anti-preferred stimuli, for the same cells as in *A*–*C. F,* ROC analysis for anti-preferred stimulus.

Figure 9

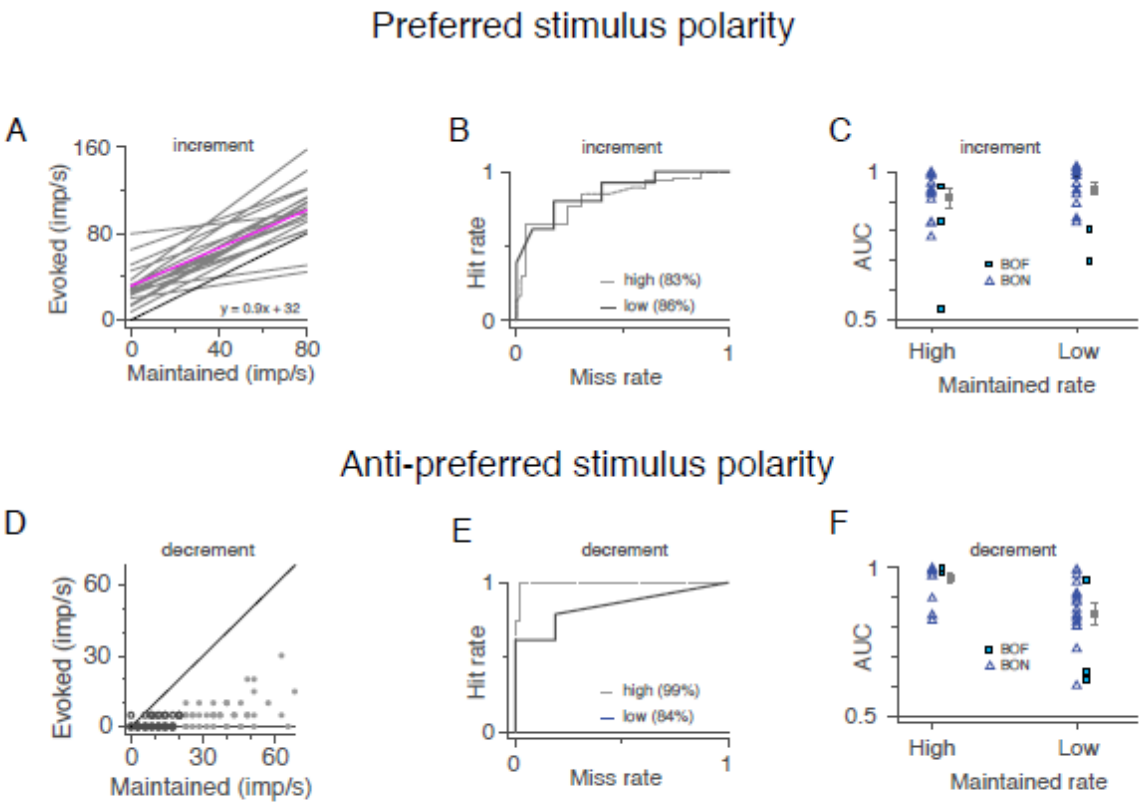

Figure 10. *A*, Example of delta-frequency spike timing analysis. Black trace (upper) is the raw LFP, the blue trace (center) is the same data band pass filtered for delta frequencies (1–4 Hz). The blue triangles represent action potential from a single K-blue on cell. *B*, Example distribution of non-uniform phase relationship between LGN cell spike rate and V1 delta waves. Histogram shows instantaneous phase taken from a Hilbert trans- form of the delta-filtered LFP at the time of each spike. The solid line is an illustration of voltage-phase relation for a single delta wave. *C*, Fraction of phase-locked cells during low and high delta periods. *D*, Polar plots of

all cells that showed significant phase-locking during high delta periods. Thick black line shows the mean vector direction.

Figure 10